Journal of Inorganic Biochemistry 174 (2017) 102–110

Contents lists available at ScienceDirect

Journal of Inorganic Biochemistry

journal homepage: www.elsevier.com/locate/jinorgbio

Anticancer activity of hydroxy- and sulfonamide-azobenzene platinum(II) complexes in cisplatin-resistant ovarian cancer cells

Katia G. Samper[a,b], Sierra C. Marker[a], Pau Bayón[b], Samantha N. MacMillan[a], Ivan Keresztes[a], Òscar Palacios[b,*], Justin J. Wilson[a,*]

[a] Department of Chemistry and Chemical Biology, Cornell University, Ithaca, NY 14853, United States
[b] Departament de Química, Facultat de Ciències, Universitat Autònoma de Barcelona, Cerdanyola del Vallès, E-08193 Barcelona, Spain

ARTICLE INFO

Keywords:
Cisplatin
Cisplatin resistance
Antitumor drug
Ovarian cancer
Azobenzene
Photodynamic therapy

ABSTRACT

The syntheses of three platinum(II) complexes bearing sulfonamide- ((*E*)-2-(4-methylphenylsulfonamido)-2′,6′-difluoroazobenzene, **HL1**) and hydroxy-azo-2,6-difluorobenzene ((*E*)-2-((2,6-difluorophenyl)diazenyl)phenol, **HL2**) bidentate ligands is described. These complexes, [Pt(**L1**)(DMSO)Cl] (**1**), [Pt(**L2**)(DMSO)Cl] (**2**), and [Pt(**L2**)$_2$] (**3**), were characterized by multinuclear NMR spectroscopy, mass spectrometry, and X-ray crystallography. Despite bearing azobenzene functional groups, none of the three complexes undergo photoisomerization. The anticancer activities of these complexes were evaluated in wild-type (A2780) and cisplatin-resistant (A2780CP70) ovarian cancer cells. All three complexes exhibited IC_{50} values below 10 μM and displayed similar activity in both A2780 and A2780CP70 cell lines, indicating that they are not cross-resistant with cisplatin. The DNA-binding properties of **1**–**3** were investigated by circular dichroism spectroscopy and by agarose gel electrophoresis. Both studies suggest that **1** and **2** form monofunctional DNA adducts.

1. Introduction

Cisplatin and its second-generation analogue carboplatin are FDA-approved chemotherapeutic drugs that are used as part of the first-line treatment for several different types of cancer [1,2]. These relatively simple coordination complexes of platinum(II) have had a significant impact on cancer survival [3]. Particularly, the cure rates of testicular cancer, once a relatively fatal disease, now exceed 80% with platinum-based chemotherapy [4,5]. While these drugs are useful for other cancer types as well, the development of resistance to cisplatin is a common phenomenon that severely hinders patient survival [6]. An additional limitation of these drugs lies in the toxic side effects that they induce [7–10], which are a consequence of their lack of cancer cell selectivity.

The use of light to activate cytotoxic agents is an approach that is employed clinically in the form of photodynamic therapy (PDT) [11]. This strategy imparts cytotoxicity selectively to regions of light irradiation, minimizing systemic toxic side effects. While most PDT agents act as sensitizers for singlet oxygen [12,13], recent research efforts have focused on the development of inorganic complexes that undergo ligand photosubstitution reactions to form cytotoxic complexes or release biologically active ligands [14–16]. Such strategies are potentially more effective than singlet oxygen sensitization because solid tumors often exist in a state of hypoxia where the low O_2 concentration makes this process ineffective.

In this study, we aimed to explore a different strategy for the development of photoactivated anticancer agents, one which uses light as a means to change the ligand configuration on the platinum(II) center to modulate the biological activity of these complexes. This approach has been successfully implemented using platinum(II) compounds bearing photoreactive 1,2-dithienylethene-containing ligands [17]. Here, we explored platinum(II) coordination complexes containing azobenzene-based ligands, which are known to undergo $E \rightarrow Z$ isomerization upon irradiation with light [18]. We hypothesized that a change in ligand configuration would alter the ability of the complex to interact with biological targets such as DNA. Additionally, azobenzene-based ligands have effectively been employed in the development of potent anticancer complexes of platinum [19,20], ruthenium [21,22], and osmium [23]. We prepared two bidentate azobenzene-based ligands, and three platinum(II) complexes. The photoreactivities of these complexes and the in vitro anticancer activities in wild-type and cisplatin-resistant ovarian cancer cell lines were investigated. Although the compounds were found to be inert to light irradiation, we have discovered that these complexes possess potent anticancer activities that are not susceptible to platinum-resistance mechanisms.

* Corresponding authors.
E-mail addresses: oscar.palacios@uab.cat (Ò. Palacios), jjw275@cornell.edu (J.J. Wilson).

http://dx.doi.org/10.1016/j.jinorgbio.2017.06.003
Received 5 April 2017; Received in revised form 13 May 2017; Accepted 12 June 2017
Available online 17 June 2017

2. Experimental

2.1. General considerations

Reactions were carried out under normal atmospheric conditions with no efforts to exclude moisture or oxygen. Solvents used were HPLC grade. The compounds (*E*)-2-(4-methylphenylsulfonamido)-2′,6′-difluoroazobenzene (**HL1**) and 2,6-difluoronitrosobenzene were synthesized as previously described [24] from commercially available reagents. The complex *cis*-[Pt(DMSO)$_2$Cl$_2$] was prepared from K$_2$PtCl$_4$, as previously reported [25].

2.2. Physical measurements

Elemental analyses were carried out by Atlantic Microlab, LLC (Norcross, Georgia, USA). NMR spectra were acquired on a 500 MHz Bruker AV III HD spectrometer equipped with a broadband Prodigy cryoprobe or on a Varian INOVA 400 MHz spectrometer. ^{1}H and ^{13}C{^{1}H} NMR spectra were referenced using residual protic solvent peaks [26], relative to tetramethylsilane (TMS) at 0 ppm. ^{195}Pt, ^{19}F{^{1}H}, and ^{15}N NMR chemical shift scales are referenced relative to Na$_2$PtCl$_6$ in D$_2$O, neat CFCl$_3$, and liquid NH$_3$, all set at 0 ppm. UV–vis spectra were acquired using an Agilent Cary 8454 UV–visible spectrophotometer. IR spectra were acquired on a Bruker Hyperion ATIR with ZnSe ATR attachment for solid powders. High-resolution mass spectra (HRMS) were obtained with an Exactive Orbitrap mass spectrometer in positive ESI or DART mode (ThermoFisher Scientific, Waltham, MA). Photoisomerization studies were carried out with continuous irradiation using a 6-watt UVP UVGL-55 handheld UV lamp at 254 nm and 365 nm.

2.3. Synthesis

2.3.1. Synthesis of (E)-2-((2,6-difluorophenyl)diazenyl)phenol (*HL2*)

To a flask containing 2,6-difluoronitrosobenzene (1.299 g, 9.08 mmol) was added acetic acid (20 mL), inducing a color change from brown to green. Then, 2-aminophenol (991 mg, 9.08 mmol) was added, and the mixture was stirred at room temperature for 2 d. The solvent was evaporated under reduced pressure, and the crude product was purified by flash column chromatography using SiO$_2$ as the stationary phase and hexanes as the mobile phase to afford **HL2** as an orange crystalline solid. (200 mg, 0.85 mmol, 9%) ^{1}H NMR (400 MHz, CDCl$_3$): δ 12.30 (s, 1H), 7.99 (d, J = 8.2 Hz, 1H), 7.44–7.32 (m, 2H), 7.12–7.03 (m, 4H). ^{13}C{^{1}H} NMR (100 MHz, CDCl$_3$): δ 156.2 (dd, J = 261.2 Hz, J = 4.1 Hz), 152.5, 138.8, 134.5, 133.6, 130.9 (t, J = 10.94 Hz), 128.9, 120.2, 118.61, 112.1 (dd, J = 23.8 Hz, J = 4.1 Hz). ^{19}F{^{1}H} NMR (376 MHz, CDCl$_3$): δ −120.41. IR (ATR, cm^{-1}): 3099 w, 3066 w, 2922 w, 2852 w, 1614 s, 1589 s, 1470 vs, 1411 s, 1358 m, 1323 w, 1289 s, 1271 s, 1227 s, 1146 s, 1111 m, 1025 vs, 818 s, 785 s, 754 vs. DART-MS (positive ion mode): m/z 235.0674 ([M + H]$^+$, calcd. 235.0677). Anal. Calcd. for C$_{12}$H$_8$F$_2$N$_2$O: C, 61.54; H, 3.44; N, 11.96. Found: C, 61.37; H, 3.61; N, 11.84.

2.3.2. Synthesis of [Pt(*L1*)Cl(DMSO)] (*1*)

Triethylamine (61.8 mg, 85.2 μL, 0.61 mmol) was added to a flask containing **HL1** (118.3 mg, 0.31 mmol) in methanol (28 mL). After stirring for 5 min, solid *cis*-[Pt(DMSO)$_2$Cl$_2$] (99.2 mg, 0.24 mmol) was added, and the mixture was heated at 45 °C for 2 h. The solution was then allowed to cool to room temperature, and the solvent was evaporated under reduced pressure. The crude material was purified by flash column chromatography (SiO$_2$, 9:1 CH$_2$Cl$_2$:EtOAc) to obtain a pink solid (43.3 mg, 0.062 mmol, 26%). ^{1}H NMR (400 MHz, CDCl$_3$): δ 7.73 (d, J = 8.25 Hz, 2H), 7.68–7.62 (m, 2H), 7.45–7.36 (m, 2H), 7.14–7.05 (m, 5H), 3.33 (s, 3H), 3.27 (s, 3H), 2.29 (s, 3H). ^{13}C{^{1}H} NMR (100 MHz, CDCl$_3$): δ 156.6 (d, J = 202 Hz), 155.3, 148.0, 142.5, 139.2, 136.8, 132.9, 132.3, 131.2 (t, J = 9.05 Hz), 129.1, 127.9, 124.5, 124.1, 112.1 (dd, J = 20.1 Hz, J = 3.5 Hz), 45.0, 44.4, 21.6. ^{19}F{^{1}H} NMR (376 MHz, CDCl$_3$): δ −119.8, −120.5. ^{195}Pt NMR (128 MHz, CDCl$_3$): δ −2378. IR (ATR, cm^{-1}): 3014 w, 2927 w, 2853 w, 1616 w, 1596 m, 1468 m, 1423 m, 1317 m, 1279 m, 1249 m, 1141 vs, 1084 s, 1018 s, 948 s, 914 s, 856 s, 764 s. UV–Vis (CH$_2$Cl$_2$): λ_{max} (ε) 260 nm (1.26 × 10^4 M^{-1}·cm^{-1}); 328 nm (5.48 × 10^3 M^{-1}·cm^{-1}); 537 nm (2.06 × 10^3 M^{-1}·cm^{-1}). HR-MS (positive ion mode): m/z 718.0134 ([M + Na]$^+$, calcd. 718.0135). Anal. Calcd. for **1**·CHCl$_3$ (C$_{22}$H$_{21}$Cl$_4$F$_2$N$_3$O$_3$PtS$_2$): C, 32.45; H, 2.60; N, 5.16. Found: C, 32.18; H, 2.46; N, 4.96.

2.3.3. Syntheses of [Pt(*L2*)Cl(DMSO)] (*2*) and [Pt(*L2*)$_2$] (*3*)

To a solution of **HL2** (24.5 mg, 0.10 mmol) and NaOH (5.5 mg, 0.14 mmol) in methanol (1.6 mL) was added a suspension of *cis*-[Pt(DMSO)$_2$Cl$_2$] (42.8 mg, 0.10 mmol) in acetone (3.2 mL). The mixture was heated at 45 °C for 2 h. After allowing the mixture to cool to room temperature, the solvent was removed under reduced pressure. The crude product was purified by flash column chromatography (SiO$_2$, gradient of 1:5 hexane:EtOAc to 100% EtOAc) to separate complex **3**, which eluted first, as a purple crystalline solid (12 mg, 0.018 mmol, 18%) and complex **2**, a red solid (47 mg, 0.086 mmol, 86%).

Complex **2**: ^{1}H NMR (500 MHz, CDCl$_3$): δ 7.74 (d, J = 8.2 Hz, 1H), 7.63 (t, J = 7.3 Hz, 1H), 7.35–7.27 (m, 1H), 7.24 (d, J = 8.5 Hz, 1H), 7.03–6.96 (m, 2H), 6.85 (t, J = 7.3 Hz, 1H), 3.48 (s, 6H). ^{13}C{^{1}H} NMR (100 MHz, CDCl$_3$): δ 156.6 (d, J = 200 Hz), 154.6, 149.4, 140.0, 137.9, 133.3, 128.5 (t, J = 10.12 Hz), 120.6, 118.6, 110.8 (dd, J = 19.0 Hz, J = 4.5 Hz), 46.0. ^{19}F{^{1}H} NMR (376 MHz, CDCl$_3$): δ −121.8. ^{195}Pt NMR (128 MHz, CDCl$_3$): δ −2430. IR (ATR, cm^{-1}): 3060 w, 3007 w, 2920 w, 2851 w, 1610 m, 1599 m, 1477 vs, 1394 s, 1307 s, 1291 s, 1250 m, 1146 s, 1009 vs, 959 m, 786 s, 753 s. UV–Vis (CH$_2$Cl$_2$): λ_{max} (ε) 302 nm, (1.05 × 10^4 M^{-1}·cm^{-1}); 496 nm, (5.68 × 10^3 M^{-1}·cm^{-1}). DART-MS (positive ion mode): m/z 542.0072 ([M + H]$^+$, calcd. 542.0080). Anal. Calcd for **2** (C$_{14}$H$_{13}$ClF$_2$N$_2$O$_2$PtS): C, 31.03; H, 2.42; N, 5.17. Found: C, 31.30; H, 2.36; N, 5.22.

Complex **3**: ^{1}H NMR (500 MHz, CDCl$_3$): δ 7.70 (d, J = 8.3 Hz, 1H), 7.58 (t, J = 7.2 Hz, 1H), 7.29 (d, J = 8.3 Hz, 1H), 7.12–7.04 (m, 1H), 6.79 (t, J = 7.3 Hz, 1H), 6.69 (m, 2H). ^{13}C{^{1}H} NMR (100 MHz, CDCl$_3$): δ 154.9 (d, J = 200 Hz), 153.9, 151.7, 143.6, 137.5, 133.7, 129.0 (t, J = 9.3 Hz), 121.9, 119.1, 112.6 (dd, J = 19.9 Hz, J = 3.64 Hz, 2C). ^{19}F{^{1}H} NMR (376 MHz, CDCl$_3$): δ −117.36. ^{195}Pt NMR (128 MHz, CDCl$_3$): δ −1006. IR (ATR, cm^{-1}): 3064 w, 2923 w, 2852 w, 1734 m, 1605 s, 1593 s, 1526 m, 1471 s, 1380 s, 1308 s, 1238 s, 1180 s, 1140 s, 1015 s, 944 s, 847 s, 779 s, 747 vs. UV–Vis (CH$_2$Cl$_2$): λ_{max} (ε) 259 nm (3.69 × 10^4 M^{-1}·cm^{-1}); 322 nm (2.11 × 10^4 M^{-1}·cm^{-1}); 426 nm (1.27 × 10^4 M^{-1}·cm^{-1}); 538 nm (7.05 × 10^3 M^{-1}·cm^{-1}); 592 nm (7.04 × 10^3 M^{-1}·cm^{-1}). DART-MS (positive ion mode): m/z 662.0763 ([M + H]$^+$, calcd. 662.0779). Anal. Calcd. for **3**·0.5EtOAc (C$_{26}$H$_{18}$F$_4$N$_4$O$_3$Pt): C, 44.26; H, 2.57; N, 7.94. Found: C, 44.54; H, 2.31; N, 8.35.

2.4. X-ray crystallography

Single crystals of **1** were grown by the slow evaporation of a solution of 1:1 CH$_2$Cl$_2$:CHCl$_3$, and crystals of **2** and **3** were grown by the slow evaporation of a solution mixture of hexane and EtOAc. These crystals were mounted on a Bruker X8 Kappa diffractometer coupled to an ApexII CCD detector with graphite-monochromated Mo Kα radiation (λ = 0.71073 Å), and cooled to 223 K under a nitrogen cold-stream during data collection. The program SHELXT was used to solve the structures via intrinsic phasing [27], which were refined on all data by full-matrix least squares with SHELXL [28]. Non-hydrogen atoms were refined anisotropically. Hydrogen atoms were placed at calculated positions using a riding model, and were refined isotropically with thermal displacement parameters constrained to be either 1.2 or 1.5 (for terminal CH$_3$) times that of the atom to which it's attached. For compound **2**, two voids with disordered electron density within the unit

Table 1
X-ray crystallographic data collection and refinement parameters for **1–3**.

	1	2	3
Formula	$C_{23}H_{22}Cl_7F_2N_3O_3S_2Pt$	$C_{14}H_{13}ClF_2N_2O_2SPt$	$C_{24}H_{14}F_4N_4O_2Pt$
Fw	933.79	541.86	661.48
Space group	$P\bar{1}$	$P2_1/m$	$Pbca$
a, Å	10.5085(6)	10.7585(4)	15.6646(17)
b, Å	10.9522(7)	23.2042(9)	15.514(2)
c, Å	15.7656(10)	10.9692(4)	18.009(2)
α, deg	83.455(3)	90	90
β, deg	81.522(3)	96.571(2)	90
γ, deg	64.594(3)	90	90
V, Å^3	1618.48(18)	2720.39(18)	4376.6(9)
Z	2	6	8
ρ_{calcd}, g·cm^{-3}	1.916	1.985	2.008
T, K	223(2)	223(2)	223(2)
μ(Mo Kα), mm^{-1}	5.085	8.025	6.477
Θ range, deg	2.062 to 30.034	1.869 to 30.033	2.166 to 28.699
Completeness to Θ (%)	99.7	99.9	99.9
Total no. of data	36,781	34,063	47,612
No. of unique data	9441	8132	5647
No. of parameters	373	337	316
R1[a] (%)	2.77	2.83	1.86
wR2[b] (%)	7.48	5.69	3.98
GOF[c]	1.082	1.036	1.018
Max, min peaks, e·Å^{-3}	1.888, −1.300	1.267, −1.451	0.398, −0.724

[a] $R_1 = \Sigma||F_o| - |F_c||/\Sigma|F_o|$ for $I > 2\sigma$.
[b] $wR_2 = \{\Sigma[w(F_o^2 - F_c^2)^2] / \Sigma[w(F_o^2)^2]\}^{1/2}$ for $I > 2\sigma$.
[c] GoF $= \{\Sigma[w(F_o^2 - F_c^2)^2] / (n - p)\}^{1/2}$, where n is the number of data and p is the number of refined parameters.

cell were modeled with the SQUEEZE algorithm [29]. These voids each occupied a volume of 170 Å^3 and accounted for the scattering contributions of 59 e$^-$, which we attribute to two disordered molecules of ethyl acetate. Additionally, two molecules of **2** were present in the asymmetric unit. One molecule lies on the general position and the other lies on a crystallographic mirror plane. Crystallographic data collection and refinement parameters are collected in Table 1.

2.5. Agarose gel electrophoresis

A stock solution of the closed supercoiled pUC19 plasmid DNA (1000 μg/mL) was used for electrophoretic mobility experiments. Solutions of pUC19 plasmid DNA (15 μg/mL) in Tris HCl (10 mM, pH 7.4) were mixed with solutions of **1–3** and cisplatin to final concentrations ranging from 0 to 125 μM (r_i = 0–0.20) in a total volume of 100 μL. Complexes **1–3** were diluted from DMF solutions and cisplatin from an aqueous solution. These samples were incubated for 16 h at 37 °C. After incubation, the samples were dialyzed using Fisher brand dialysis membrane (regenerated cellulose) with a molecular weight cutoff of 6000–8000 Da against 1.0 L of TE (10 mM Tris HCl, 1 mM EDTA, pH 7.4) buffer for 2–3 h to remove unbound platinum. The dialyzed samples were analyzed using a NanoDrop 1000 (Thermo Scientific, Waltham, MA) to verify plasmid concentration (μg/mL) and a Perkin Elmer PinAAcle 900z graphite furnace atomic absorption spectrometer (GFAAS) to determine bound platinum concentration. The ratio of platinum atoms to nucleotides from these measurements was used to determine the r_b value. Table S1 (Supplementary data) shows the r_b values obtained after dialysis at a given r_f value. A 10 μL quantity of each sample was mixed with 3 μL of 5 × Orange DNA Loading Dye, and 10 μL of this mixture was loaded on a slab of 1% agarose gel. The agarose gel was subjected to electrophoresis in 0.5 × TAE pH 8 buffer at 80 V for 1 h. The gel was then removed from the electrophoresis tank and mixed gently in a solution containing GelStar Nucleic Acid (Lonza) stain for 1 h. The DNA bands were visualized with a ChemiDoc MP Imaging System (BioRad) by fluorescence.

2.6. Circular dichroism measurements

Circular dichroism (CD) measurements were performed using a JASCO spectropolarimeter (model J-715, JASCO, Groß-Umstadt, Germany) controlled with the J700 software, (JASCO, Groß-Umstadt, Germany). Samples were analyzed in 1-cm capped quartz cuvettes, and the temperature was maintained at 25 °C with a Peltier PTC-351S holder (TE Technology, Traverse City, MI, USA). Spectra were processed using the GRAMS 32 software (Thermo Fisher Scientific, Waltham, MA, USA). Stock solutions of calf thymus DNA (3.5 mM, Sigma Aldrich), Tris HCl (400 mM), and platinum complexes (15 mM) were used to prepare the different samples. The DNA concentration was determined spectrophotometrically at 260 nm by using the molar absorptivity value of 6600 M^{-1}·cm^{-1} per nucleotide. Cisplatin and **1–3** were incubated at 37 °C for 16 h with 50 μM DNA in pH 7.4 10 mM Tris HCl at platinum to nucleotide ratios (r_i) of 0.2, 0.5, and 1 prior to analysis by CD. Each sample was scanned twice in a range of wavelengths between 230 and 310 nm. The ellipticity values are given in millidegrees (mdeg).

2.7. Cell culture and cytotoxicity assays

A2780 (ovarian cancer) and A2780CP70 (cisplatin-resistant ovarian cancer) cell lines [30] were provided by the Cell Culture Facility of Fox Chase Cancer Center (Philadelphia, PA). These cells were cultured as monolayers with Roswell Park Memorial Institute (RPMI)-1640 culture media supplemented with 10% fetal bovine serum in a humidified incubator at 37 °C with an atmosphere of 5% CO_2. Cells were passed at 80–90% confluence, using trypsin/EDTA. Cells were tested monthly for mycoplasma contamination with the PlasmoTest™ mycoplasma detection kit from InvivoGen.

Cisplatin was dissolved in phosphate-buffered saline (PBS, pH 7.4) to prepare a 2 mM stock solution. Stock solutions of ligands **HL1** and **HL2** were prepared as 10 mM solutions in DMSO. The platinum complexes **1–3** were also prepared as 10 mM stock solutions in either DMSO or DMF. Cells were grown to 80–90% confluence, detached with trypsin/EDTA, seeded in 96-well plates at 4000 cells/well in 100 μL of growth media, and incubated for 24 h. The medium was removed and replaced with fresh medium (200 μL) containing varying concentrations of either cisplatin, **HL1**, **HL2**, or **1–3**. The maximum DMSO and DMF content of these solutions did not exceed 1% and 0.25%, respectively. After incubating for 72 h, the medium was removed from the wells, and 3(4,5-dimethylthiazol-2-yl)-2,5-tetrazolium bromide (MTT) in RPMI (200 μL, 1 mg/mL) was added. After 4 h, the MTT/RPMI solution was removed, and the formazan crystals were dissolved in 200 μL of an 8:1 mixture of DMSO and pH 10 glycine buffer. The absorbance at 570 nm in each well was measured using a BioTek Synergy HT plate reader. Cell viability was determined by normalizing the absorbance of the treated wells to untreated wells. The concentration of the compound versus % viability was plotted to produce the dose-response curves, which were analyzed using a logistic sigmoid function fit with MagicPlot Pro software. The reported IC_{50} values are the average of three independent experiments with six replicates per concentration level.

3. Results and discussion

3.1. Synthesis and characterization

The synthetic scheme for the azobenzene ligands **HL1** and **HL2** is shown in Scheme 1. The syntheses commenced from commercially available 2,6-difluoroaniline, which was oxidized with oxone to yield 2,6-difluoronitrosobenzene. The reaction of this reagent with *N*-tosyl-*o*-phenylenediamine in acetic acid under reflux affords **HL1** [24]. The

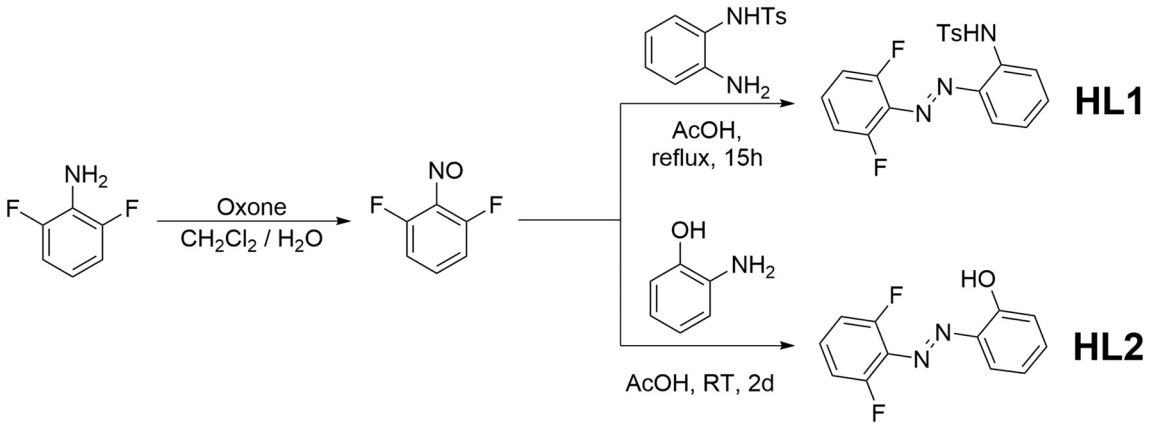

Scheme 1. Synthesis of **HL1** and **HL2**.

ligand **HL2** was obtained from the reaction of 2-aminophenol and 2,6-difluoronitrosobenzene under conditions similar to those used for **HL1**. These ligands were characterized by ^{1}H, $^{13}C\{^{1}H\}$, and $^{19}F\{^{1}H\}$ NMR spectroscopy after purification by column chromatography.

The reactions of **HL1** and **HL2** with *cis*-$[Pt(DMSO)_2Cl_2]$ were investigated (Scheme 2). The reaction with **HL1** afforded primarily a single platinum-containing product as a pink solid, **1**. From the reaction of **HL2**, two compounds could be isolated and separated by column chromatography; a red solid, **2**, was the major product, and a purple solid, **3**, was the minor product. Notably, when the reaction was carried out using lower concentrations, the yield of **2** increased. Mass spectrometry was consistent with formulation of the complexes as [Pt(**L1**)Cl(DMSO)] (**1**), [Pt(**L2**)Cl(DMSO)] (**2**), and [Pt(**L2**)$_2$] (**3**), as molecular ion peaks with the expected masses and isotopic patterns corresponding to $[M + H]^+$ and $[M + Na]^+$ were observed. The ^{195}Pt NMR chemical shifts of complexes **1**–**3** are −2378, −2430, and −1006 ppm, respectively, all falling within the range expected for platinum in the +2 oxidation state [31,32]. The chemical shift of **3** is consistent with an N_2O_2 coordination environment [31]. The chemical shifts of **1** and **2** are upfield of **3** by > 1000 ppm, which reflects coordination of the soft S-donor DMSO ligand to these platinum centers [33].

The ligands **L1**$^-$ and **L2**$^-$ can coordinate to metal ions in two different manners, forming either a five-membered or six-membered chelate ring (Scheme 3). The assignment of chelate rings for related dihydroxydiarylazo platinum(II) compounds was previously established with ^{15}N NMR spectroscopy [34]. To determine the chelate ring forms in **2**, we employed 2-D $^{1}H,^{15}N$-HMBC and $^{19}F,^{15}N$-HMBC NMR spectroscopic experiments (Fig. 1). For **HL2**, two cross peaks were observed in the $^{1}H,^{15}N$-HMBC spectrum corresponding to a correlation between N2 and the *ortho* CH hydrogen (^{15}N δ = 531 ppm) and between N1 and the *ortho* OH hydrogen (^{15}N δ = 443 ppm). The latter correlation is most likely mediated via a hydrogen bond. Similar correlations resulting from strong hydrogen bonds have been observed in $^{1}H,^{31}P$-HMBC spectra [35]. The $^{19}F,^{15}N$-HMBC NMR spectra showed that the fluorine atoms correlate to both nitrogen nuclei. Upon coordination to platinum(II), the $^{1}H,^{15}N$-HMBC spectrum of **2** displays a single cross-peak arising from the correlation between N2 and an *ortho* CH (^{15}N δ = 461 ppm). The cross-peak from the OH group is no longer present because this group is deprotonated when coordinated to platinum(II). The $^{19}F,^{15}N$-HMBC NMR spectrum, however, only shows a single cross-peak as well. No correlation with N1 is observed. The loss of this

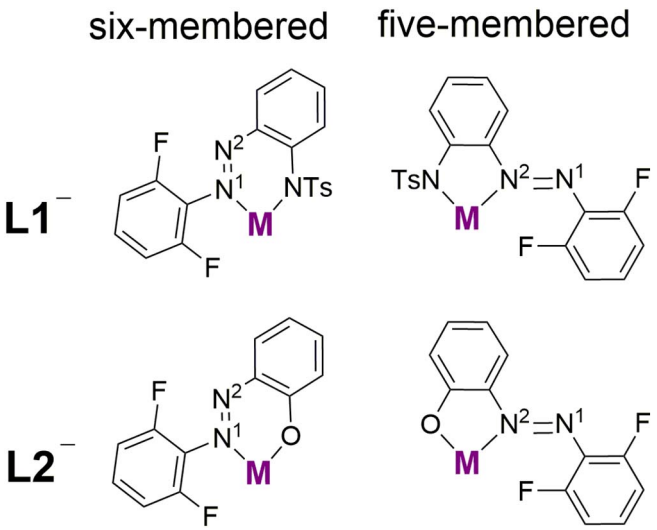

Scheme 3. Five- and six-membered chelate rings possible for **L1**$^-$ and **L2**$^-$.

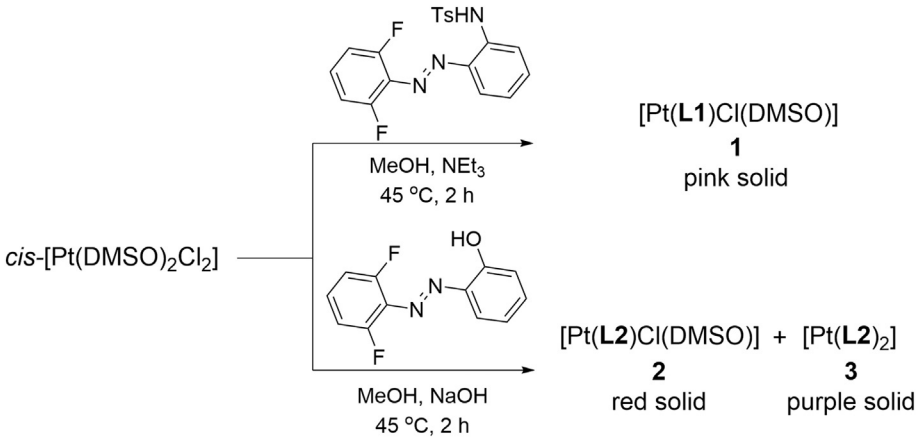

Scheme 2. Reactions of *cis*-$[Pt(DMSO)_2Cl_2]$ with **HL1** and **HL2**.

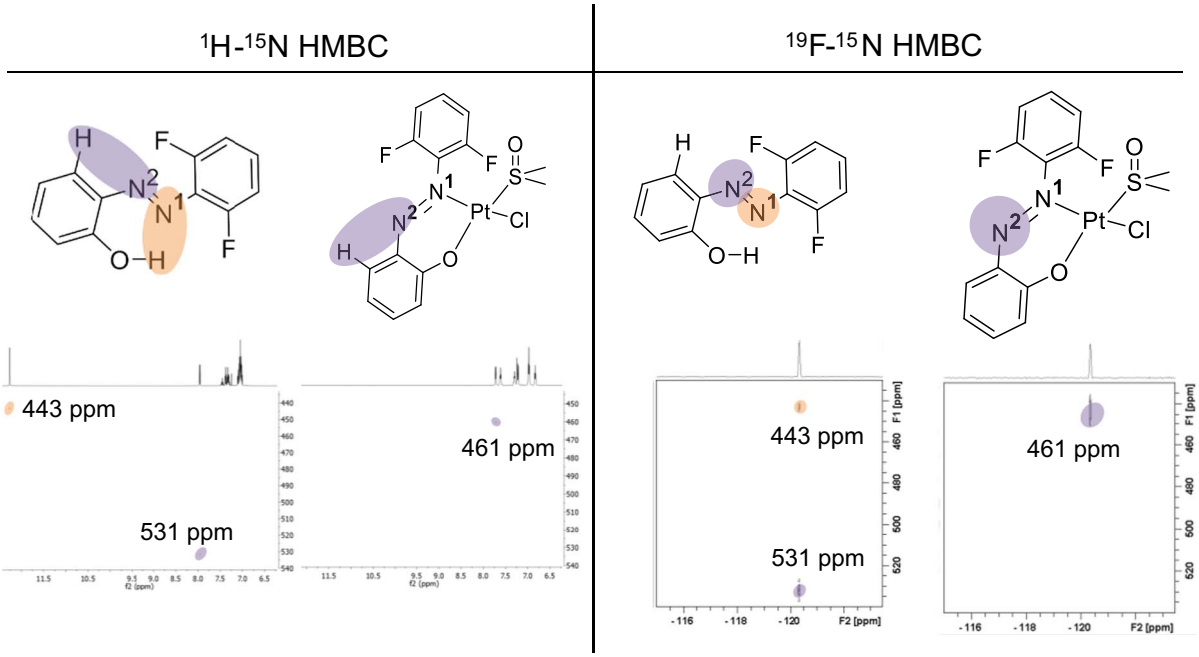

Fig. 1. 2-D ^{1}H,^{15}N-HMBC and ^{19}F,^{15}N-HMBC NMR spectroscopy of **HL2** and **2** in $CDCl_3$ at 25 °C.

correlation most likely results from the increase in the relaxation rate of this nitrogen nucleus due to direct coordination to the platinum center. The platinum center relaxes the coordinated ^{15}N nucleus effectively via chemical shift anisotropy, a dominant relaxation mechanism for heavy nuclei. Therefore, these experiments indicate that the platinum is coordinated to N1, forming a six-membered ring.

3.2. X-ray crystal structures

Complexes **1–3** were characterized structurally by X-ray crystallography, as shown in Figs. 2–4. For **2**, two molecules are present in the asymmetric unit; both are similar with respect to interatomic distances and angles. All three structures reveal square planar coordination geometries, as expected for complexes of platinum(II). As predicted by the 2-D NMR experiments, ligands **L1**$^-$ and **L2**$^-$ form six-membered chelate rings in all three complexes as well. By contrast, ruthenium and rhodium complexes bearing related sulfonamide-diazo donor ligands exclusively form five-membered chelate rings [24,36]. Complexes **1** and **2** contain a molecule of DMSO coordinated through the sulfur donor and chloride ligand in addition to **L1**$^-$ and **L2**$^-$, respectively. In both structures, the chloride ligand sits *trans* to the coordinated diazo nitrogen donor. The Pt–S(DMSO) distance is longer in complex **1** (2.237 Å) than in **2** (2.225 and 2.227 Å), presumably due to the greater *trans* influence of the sulfonamide donor compared to the phenolate donor. Additionally, the chelate ring geometry found in **1** is substantially different than that found in **2**. In **2**, this six-membered chelate

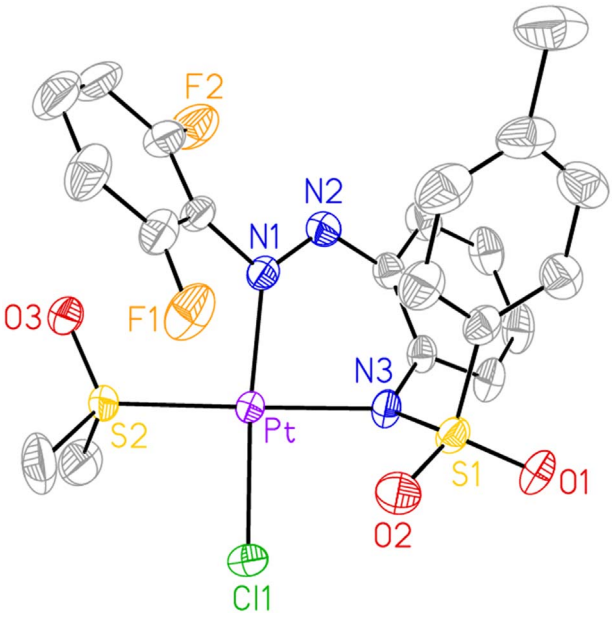

Fig. 2. X-ray crystal structure of **1**. Ellipsoids are drawn at the 50% probability level and hydrogen atoms are omitted for clarity. Selected interatomic distances (Å): Pt–Cl1 2.2967(9), Pt–S2 2.2368(7), Pt–N1 2.018(3), Pt–N3 2.037(2). Selected angles (°): N1–Pt–N3 84.99(10), N1–Pt–S2 94.46(7), N3–Pt–S2 174.31(8), N1–Pt–Cl1 175.27(7), N3–Pt–Cl1 90.29(8), S2–Pt–Cl1 90.27(3).

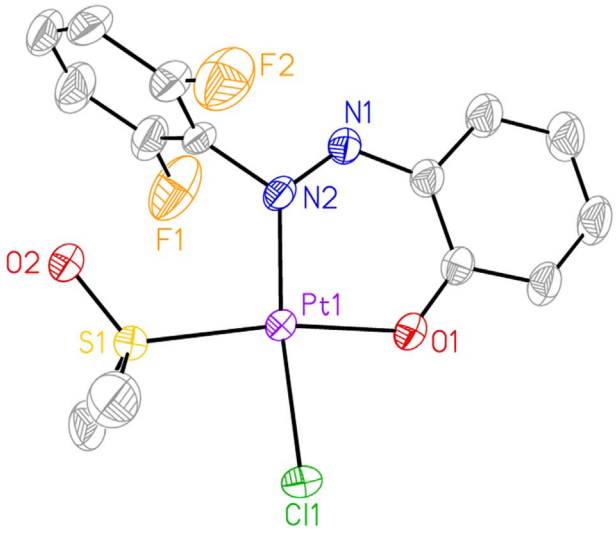

Fig. 3. X-ray crystal structure of one of the molecules of **2** present in the asymmetric unit. Ellipsoids are drawn at the 50% probability level and hydrogen atoms are omitted for clarity. Selected interatomic distances (Å): Pt1–O1 1.993(2), Pt1–N2 2.005(3), Pt1–S1 2.2248(9), Pt1–Cl1 2.3105(9). Selected angles (°): O1–Pt1–N2 90.31(10), O1–Pt1–S1 170.58(7), N2–Pt1–S1 99.04(8), O1–Pt1–Cl1 83.25(7), N2–Pt1–Cl1 173.15(8), S1–Pt1–Cl1 87.46(3).

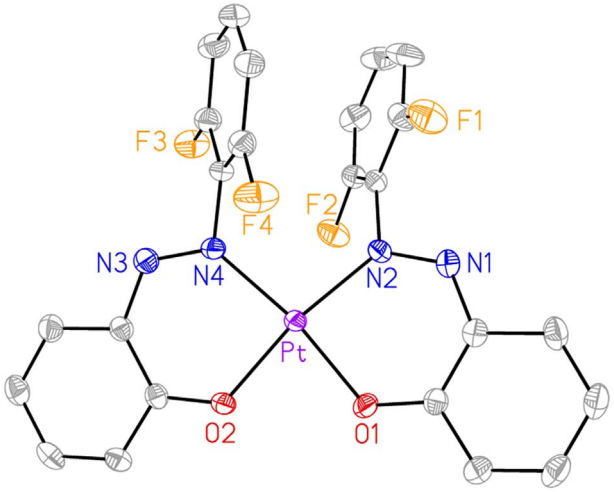

Fig. 4. X-ray crystal structure of **3**. Ellipsoids are drawn at the 50% probability level and hydrogen atoms are omitted for clarity. Selected interatomic distances (Å): Pt–O2 1.9866(16), Pt–N4 1.9910(19), Pt–O1 1.9916(15), Pt–N2 1.9997(19). Selected angles (°): O2–Pt–N4 90.32(7), O2–Pt–O1 80.64(7), N4–Pt–O1 170.70(8), O2–Pt–N2 170.38(7), N4–Pt–N2 99.16(8), O1–Pt–N2 89.94(7).

ring is planar, as reflected by the fact that one molecule in the asymmetric unit resides on a crystallographic mirror plane. The N–Pt–O angle in complex **2** is 90°. By contrast, the chelate ring in **1** attains a boat conformation. As a result, the N1–Pt–N3 angle is 85°, deviating substantially from the ideal 90° angle for a square planar complex.

The structure of complex **3** (Fig. 4) reveals two $\mathbf{L2}^-$ ligands coordinated to the central platinum(II) ion. The two six-membered chelate rings, like those in **2**, are nearly planar and give rise to N–Pt–O angles of 90°. The two $\mathbf{L2}^-$ ligands are arranged such that the nitrogen and oxygen donor atoms of the two ligands reside in a *cis* configuration. This arrangement of the ligands gives rise to a π-stacking interaction between 2,6-difluorophenyl substituents (centroid–centroid distance 3.25 Å), which may stabilize this isomer over the *trans* isomer. The Pt–N and Pt–O interatomic distances are in the expected range, falling just under 2 Å. The crystal structure of a related platinum(II) complex of analogous ligands, where the 2,6-difluorophenyl groups are tosyl groups, has been reported [37]. This structure also reveals the platinum (II) complex to be in the *cis* configuration and shows a π-stacking interaction between the tosyl groups, indicating that this structure type may be general for platinum(II) complexes with this class of ligands.

3.3. Photophysical properties

Because azobenzene derivatives are known to undergo photoisomerization reactions [38], the photophysical properties of **HL2** and **1–3** were investigated. The photophysical properties of **HL1** were previously reported [24]. This ligand undergoes efficient photoisomerization from the *E* to *Z* isomer upon irradiation with light at 315 nm [24]. By contrast, **HL2** showed no sign of photoisomerization when irradiated at either 365 or 254 nm. The lack of photoreactivity of 2-hydroxyazobenzenes has been documented before [39]. The intramolecular hydrogen bonding between the ortho-hydroxy group and a diazo nitrogen atom inhibits photoisomerization, giving rise to excited state intramolecular proton transfer as an alternative photoreaction [39].

The absorbance maxima and molar absorptivities of the platinum(II) complexes **1–3** are collected in Table 2 and shown in Fig. 5. Low-energy features ranging from 496 to 600 nm in the complexes are assigned as metal-to-ligand charge transfer (MLCT) transitions and high-energy features at wavelengths < 350 nm are assigned as intraligand π–π* transitions. Irradiation of the three complexes with 254 and 365 nm light failed to induce photoisomerization. When related ligands, however, are coordinated to ruthenium or rhodium, photoisomerization

Table 2
Absorbance maxima and molar absorptivities for **HL2** and **1–3** in CH_2Cl_2.

Compound	λ_{max}, nm (ε, $M^{-1}\cdot cm^{-1}$)
HL2	320 (18,620), 384 (8260)
1	328 (5480), 537 (2060)
2	302 (10,480), 496 (5680)
3	322 (21,130), 426 (12,720), 538 (7050), 592 (7040)

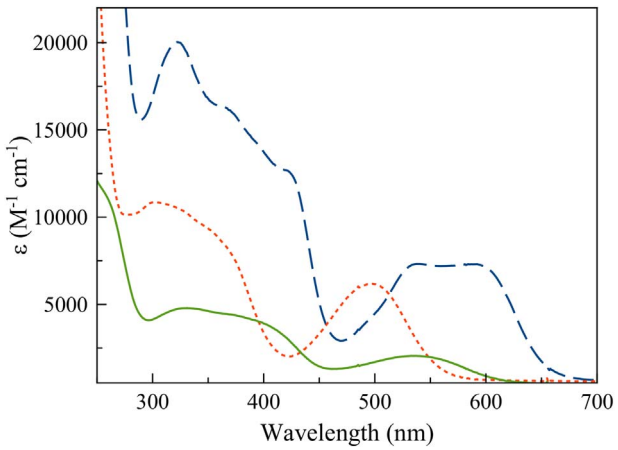

Fig. 5. UV–vis absorbance spectra of **1** (green solid), **2** (red short dash), and **3** (blue long dash) in CH_2Cl_2 at 25 °C.

occurs readily [24,36,40]. A key difference between these ruthenium and rhodium complexes and the platinum(II) complexes studied here is the nature of the chelate ring. Five-membered rings are observed for the ruthenium and rhodium complexes, whereas six-membered rings are present in **1–3**. The six-membered chelate rings effectively lock the azobenzene group in the *E* configuration. Photoisomerization in these complexes would require partial ligand dissociation to allow rotation about the N–N bond.

3.4. In vitro anticancer activity

The in vitro anticancer activities of the platinum(II) complexes and free ligands were evaluated in wild-type (A2780) and cisplatin-resistant (A2780CP70) ovarian cancer cell lines [30] (Table 3). Cisplatin was used as a positive control in these studies. Consistent with the platinum-resistant phenotype of the A2780CP70 cell lines, the IC_{50} value of cisplatin in this cell line is 28.6 times larger than that found in the wild-type cell line A2780. Although the ligand **HL2** is only moderately cytotoxic, **HL1** exhibits IC_{50} values in the micromolar range and is equally effective in both resistant and wild-type cells. Because DMSO is known

Table 3
IC_{50} values of ligands **HL1** and **HL2** and **1–3** in A2780 and A2780CP70 cell lines.

Samples	Solubilizing solvent	IC_{50} (μM)		RF[a]
		A2780	A2870CP70	
HL1	DMSO	7 ± 2	7.5 ± 0.1	1.1
HL2	DMSO	51 ± 4	66 ± 3	1.3
1	DMSO	1.0 ± 0.3	2.7 ± 0.6	2.7
1	DMF	0.43 ± 0.05	0.8 ± 0.1	1.9
2	DMSO	3.4 ± 0.7	10 ± 3	2.8
2	DMF	1.60 ± 0.09	3.2 ± 0.3	2.0
3	DMSO	6.5 ± 0.1	7.0 ± 0.1	1.1
3	DMF	2.7 ± 0.9	3.1 ± 0.6	1.1
Cisplatin	PBS	0.18 ± 0.07	5 ± 1	28.6

[a] RF = resistance factor, the ratio of the IC_{50} values measured for the resistant and wild-type cell lines.

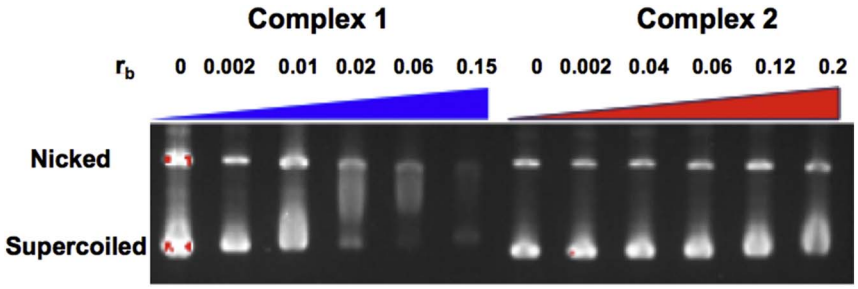

Fig. 6. Agarose (1%) gel electrophoresis of a pUC19 plasmid in the presence of **1** (left lanes) and **2** (right lanes) at different r_b values.

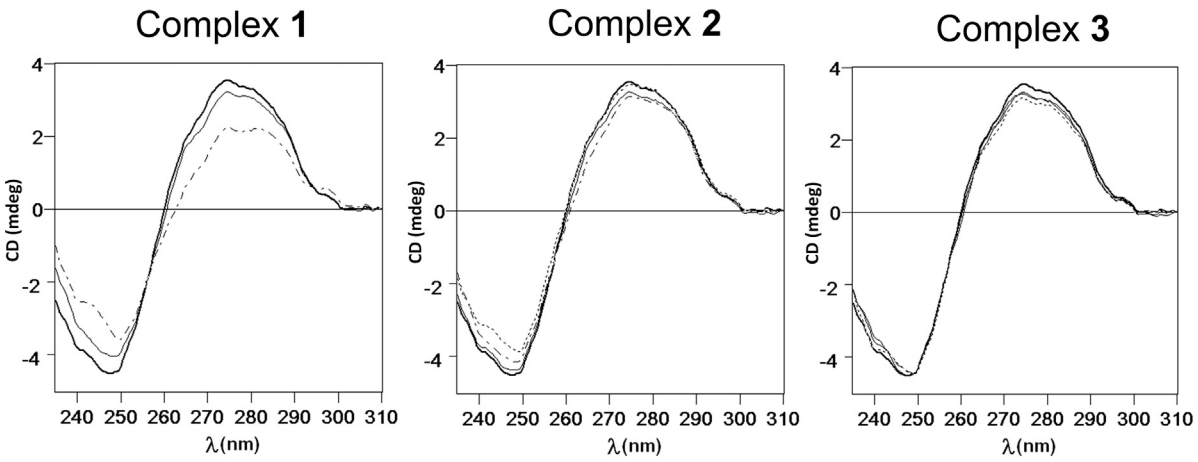

Fig. 7. CD spectra of calf-thymus DNA in the presence of **1–3** in pH 7.4 TrisCl buffer. r_i([Complex]/[nucleotide]): $r_i = 0$ (black solid line), $r_i = 0.2$ (solid grey line), $r_i = 0.5$ (long dash line), $r_i = 1$ (short dash line).

to significantly impact the activity of metal-based anticancer agents [41,42], we explored the use of both DMSO and DMF as solubilizing agents for **1–3**. Like **HL1**, all of the platinum complexes tested with either DMSO or DMF give rise to IC_{50} values that are < 10 μM, signifying potent in vitro anticancer activity. The IC_{50} values measured in the presence of DMSO were approximately 2–3 times larger than those measured using DMF. For comparison, the IC_{50} value of cisplatin dissolved in DMSO is sixty times greater than its IC_{50} value in aqueous buffer [41]. Therefore, we conclude that DMSO has only a minor effect on the anticancer activity of these complexes. The ratio of the IC_{50} values in the cisplatin-resistant and wild-type cell lines, or the resistance factors (RF), for **1–3** are all < 3, substantially smaller than the value of 28.6 measured for cisplatin. These results indicate that the azobenzene platinum(II) complexes studied here are not cross-resistant with cisplatin. This lack of cross-resistance may signify a novel or distinct mechanism of action of these complexes relative to cisplatin and carboplatin.

3.5. DNA-binding studies

Because the conventional platinum-based drugs induce their anticancer activity by covalently binding to DNA, we investigated the abilities of the azobenzene platinum(II) complexes **1–3** to interact with DNA. Cisplatin-DNA adducts result in unwinding of double-helical DNA [43], a phenomenon that is reflected by the reduction of the electrophoretic mobility of supercoiled closed circular plasmids bearing such adducts [44]. The degree of electrophoretic mobility reduction is related to the amount of unwinding in the double helix that is induced per platinum-DNA adduct. This unwinding angle, which depends on the nature of the platinum-DNA adduct, can be determined by the amount of platinum per nucleotide (r_b) required to retard the mobility of the supercoiled form to match that of the relaxed or nicked form [44]. Bifunctional platinum-DNA intrastrand crosslinks induce unwinding angles that range from 10 to 15°, whereas those for monofunctional adducts are < 8%. Irreversible covalent binding of **1** and **2** to DNA was verified by dialysis of the samples after incubation, which revealed that significant quantities of platinum remained bound to the plasmid. By contrast, dialysis of plasmid samples incubated with **3** led to complete loss of the platinum from the samples, indicating that this compound does not covalently bind to DNA. This result is expected because **3** does not bear any labile ligands that could exchange for a nucleobase ligand on DNA. Analysis of the plasmid samples with adducts of **1** and **2** revealed only minor unwinding of the double helix (Fig. 6). For **1**, unwinding is only apparent at r_b values of > 0.06, whereas for **2** no significant unwinding is observed up to an r_b of 0.2. Based on these experiments and the known superhelical density for pUC19 [44], it is estimated that the unwinding angle induced by **1** is < 10°, and the angle is < 5° for **2**. Both of these small unwinding angles are consistent with a monofunctional DNA-binding mode for these complexes [45].

The changes in the CD spectrum of DNA induced by platinum compounds reflect the nature of their interactions. Monofunctional platinum adducts give rise to only minor changes in the CD spectra, whereas those for bifunctional adducts are more dramatic [46]. When **2** and **3** were incubated at platinum to nucleotide ratios up to 1 with calf thymus DNA, only minor changes in the CD spectra were observed (Fig. 7). For **1**, the changes are more pronounced at similar ratios. The changes, however, are still not as marked as expected from bifunctional platinum DNA adducts [46]. For example, cisplatin leads to a significant increase in the CD feature at 280 nm at the much smaller r_b value of 0.10 [47]. Therefore, these CD studies, like the plasmid studies, are consistent with **1** and **2** binding to DNA in a monofunctional manner.

4. Conclusions

Three platinum(II) complexes bearing azobenzene-based ligands were synthesized and characterized. Because these compounds form six-membered chelate rings with these ligands, no photoisomerization

occurs. The ligands in this binding mode are locked into the *E* conformation by coordination to the platinum(II) centers. Nevertheless, these non-traditional platinum(II) compounds are cytotoxic in ovarian cancer cell lines. Importantly, they exhibit nearly equal activity against cisplatin-resistant and wild-type ovarian cancer cell lines, suggesting that they operate via a novel mechanism of action. DNA-binding studies suggest that **3**, which has no labile binding sites, does not interact with and distort DNA strongly. Compounds **1** and **2**, which bear chloride and DMSO ligands, weakly distort DNA in a manner that is consistent with the formation of monofunctional adducts. Therefore, **1** and **2** represent new members of the growing class of potent monofunctional platinum (II) anticancer agents [48,49].

Abbreviations

CD	circular dichroism
DMF	*N*,*N*-dimethylformamide
DMSO	dimethylsulfoxide
EDTA	ethylenediamine tetraacetic acid
GFAAS	graphite furnace atomic absorption spectroscopy
HRMS	high-resolution mass spectrometry
HL1	(*E*)-2-(4- methylphenylsulfonamido)-2′,6′-difluoroazobenzene
HL2	(*E*)-2-((2,6-difluorophenyl)diazenyl)phenol
IC_{50}	50% growth inhibitory concentration
MLCT	metal-to-ligand charge transfer
MTT	3-(4,5-dimethylthiazol-2-yl)-2,5-diphenyltetrazolium bromide
PBS	phosphate-buffered saline
PDT	photodynamic therapy
RF	resistance factor
RPMI-1640	Roswell Park Memorial Institute 1640 culture media
TAE	Tris, acetic acid, EDTA
Tris	tris(hydroxymethyl)aminomethane

Acknowledgements

Cornell University is thanked for supporting this research through start-up funding. Katia G. Samper acknowledges Departament de Química from UAB for PIF scholarship and UAB for the grant “short stay for research PIF-UAB 2016”. OP, PB, and KGS also thank the financial support from MINECO-FEDER (Projects BIO2015-67358-C2-2-P and CTQ2015-70371-REDT). This research made use of the NMR facility and the Cornell Center for Material Research (CCMR) at Cornell University, which are supported by the NSF under award numbers CHE-1531632 and DMR-1120296, respectively.

Appendix A. Supplementary data

CCDC 1540533–1540535 contains the supplementary crystallographic data for 1–3, respectively. These data can be obtained free of charge The Cambridge Crystallographic Data Centre via www.ccdc.cam.ac.uk/data_request/cif. Supplementary data associated with this article can be found, in the online version, at http://dx.doi.org/10.1016/j.jinorgbio.2017.06.003.

References

[1] F.M. Muggia, Recent updates in the clinical use of platinum compounds for the treatment of gynecologic cancers, Semin. Oncol. 31 (2004) 17–24, http://dx.doi.org/10.1053/j.seminoncol.2004.11.005.
[2] C.P. Belani, Recent updates in the clinical use of platinum compounds for the treatment of lung, breast, and genitourinary tumors and myeloma, Semin. Oncol. 31 (2004) 25–33, http://dx.doi.org/10.1053/j.seminoncol.2004.11.005.
[3] T.C. Johnstone, K. Suntharalingam, S.J. Lippard, The next generation of platinum drugs: targeted Pt(II) agents, nanoparticle delivery, and Pt(IV) prodrugs, Chem. Rev. 116 (2016) 3436–3486, http://dx.doi.org/10.1021/acs.chemrev.5b00597.
[4] L.H. Einhorn, Curing metastatic testicular cancer, Proc. Natl. Acad. Sci. U. S. A. 99 (2002) 4592–4595, http://dx.doi.org/10.1073/pnas.072067999.
[5] J.R.W. Masters, B. Köberle, Curing metastatic cancer: lessons from testicular germ-cell tumours, Nat. Rev. Cancer 3 (2003) 517–525, http://dx.doi.org/10.1038/nrc1120.
[6] L.R. Kelland, S.Y. Sharp, C.F. O'Neill, F.I. Raynaud, P.J. Beale, I.R. Judson, Mini-review: discovery and development of platinum complexes designed to circumvent cisplatin resistance, J. Inorg. Biochem. 77 (1999) 111–115, http://dx.doi.org/10.1016/S0162-0134(99)00141-5.
[7] N.E. Madias, J.T. Harrington, Platinum nephrotoxicity, Am. J. Med. 65 (1978) 307–314, http://dx.doi.org/10.1016/0002-9343(78)90825-2.
[8] I.C.S. Kennedy, B.M. Fitzharris, B.M. Colls, C.H. Atkinson, Carboplatin is ototoxic, Cancer Chemother. Pharmacol. 26 (1990) 232–234, http://dx.doi.org/10.1007/BF02897206.
[9] J.T. Hartmann, H.-P. Lipp, Toxicity of platinum compounds, Expert. Opin. Pharmacother. 4 (2003) 889–901, http://dx.doi.org/10.1517/14656566.4.6.889.
[10] T. Langer, A. am Zehnhoff-Dinnesen, S. Radtke, J. Meitert, O. Zolk, Understanding platinum-induced ototoxicity, Trends Pharmacol. Sci. 34 (2013) 458–469, http://dx.doi.org/10.1016/j.tips.2013.05.006.
[11] D.E.J.G.J. Dolmans, D. Fukumura, R.K. Jain, Photodynamic therapy for cancer, Nat. Rev. Cancer 3 (2003) 380–387, http://dx.doi.org/10.1038/nrc1071.
[12] M.C. DeRosa, R.J. Crutchley, Photosensitized singlet oxygen and its applications, Coord. Chem. Rev. 234 (2002) 351–371, http://dx.doi.org/10.1016/S0010-8545(02)00034-6.
[13] C.A. Robertson, D.H. Evans, H. Abrahamse, Photodynamic therapy (PDT): a short review on cellular mechanisms and cancer research applications for PDT, J. Photochem. Photobiol. B Biol. 96 (2009) 1–8, http://dx.doi.org/10.1016/j.jphotobiol.2009.04.001.
[14] N.J. Farrer, L. Salassa, P.J. Sadler, Photoactivated chemotherapy (PACT): the potential of excited-state d-block metals in medicine, Dalton Trans. (2009) 10690–10701, http://dx.doi.org/10.1039/b917753a.
[15] E.C. Glazer, Light-activated metal complexes that covalently modify DNA, Isr. J. Chem. 53 (2013) 391–400, http://dx.doi.org/10.1002/ijch.201300019.
[16] J.D. Knoll, C. Turro, Control and utilization of ruthenium and rhodium metal complex excited states for photoactivated cancer therapy, Coord. Chem. Rev. 282–283 (2015) 110–126, http://dx.doi.org/10.1016/j.ccr.2014.05.018.
[17] A. Presa, R.F. Brissos, A.B. Caballero, I. Borilovic, L. Korrodi-Gregório, R. Pérez-Tomás, O. Roubeau, P. Gamez, Photoswitching the cytotoxic properties of platinum (II) compounds, Angew. Chem. Int. Ed. 54 (2015) 4561–4565, http://dx.doi.org/10.1002/anie.201412157.
[18] W. Szymański, J.M. Beierle, H.A.V. Kistemaker, W.A. Velema, B.L. Feringa, Reversible photocontrol of biological systems by the incorporation of molecular photoswitches, Chem. Rev. 113 (2013) 6114–6178, http://dx.doi.org/10.1021/cr300179f.
[19] K. Mitra, S. Patil, P. Kondaiah, A.R. Chakravarty, 2-(Phenylazo)pyridineplatinum (II) catecholates showing photocytotoxicity, nuclear uptake, and glutathione-triggered ligand release, Inorg. Chem. 54 (2015) 253–264, http://dx.doi.org/10.1021/ic502317z.
[20] M.K. Raza, K. Mitra, A. Shettar, U. Basu, P. Kondaiah, A.R. Chakravarty, Photoactive platinum(II) β-diketonates as dual action anticancer agents, Dalton Trans. 45 (2016) 13234–13243, http://dx.doi.org/10.1039/C6DT02590K.
[21] S.J. Dougan, M. Melchart, A. Habtemariam, S. Parsons, P.J. Sadler, Phenylazopyridine and phenylazo-pyrazole chlorido ruthenium(II) arene complexes: arene loss, aquation, and cancer cell cytotoxicity, Inorg. Chem. 45 (2006) 10882–10894, http://dx.doi.org/10.1021/ic061460h.
[22] S.J. Dougan, A. Habtemariam, S.E. McHale, S. Parsons, P.J. Sadler, Catalytic organometallic anticancer complexes, Proc. Natl. Acad. Sci. U. S. A. 105 (2008) 11628–11633, http://dx.doi.org/10.1073/pnas.0800076105.
[23] Y. Fu, A. Habtemariam, A.M.B.H. Basri, D. Braddick, G.J. Clarkson, P.J. Sadler, Structure–activity relationships for organometallic osmium arene phenylazopyridine complexes with potent anticancer activity, Dalton Trans. 40 (2011) 10553–10562, http://dx.doi.org/10.1039/c1dt10937e.
[24] C. Deo, N. Bogliotti, R. Métivier, P. Retailleau, J. Xie, Photoswitchable arene ruthenium complexes containing *o*-sulfonamide azobenzene ligands, Organometallics 34 (2015) 5775–5784, http://dx.doi.org/10.1021/acs.organomet.5b00871.
[25] V.Y. Kukushkin, A.J.L. Pombeiro, C.M.P. Ferreira, L.I. Elding, R.J. Puddephatt, Dimethylsulfoxide complexes of platinum(II): $K[PtCl_3(Me_2SO)]$, *cis*-$[PtCl_2L(Me_2SO)]$ (L = Me_2SO, MeCN), $[PtCl(\mu\text{-}Cl)(Me_2SO)]_2$, and $[Pt(Me_2SO)_4](CF_3SO_3)_4$, Inorg. Synth. 33 (2002) 189–196, http://dx.doi.org/10.1002/0471224502.ch4.
[26] G.R. Fulmer, A.J.M. Miller, N.H. Sherden, H.E. Gottlieb, A. Nudelman, B.M. Stoltz, J.E. Bercaw, K.I. Goldberg, NMR chemical shifts of trace impurities: common laboratory solvents, organics, and gases in deuterated solvents relevant to the organometallic chemist, Organometallics 29 (2010) 2176–2179, http://dx.doi.org/10.1021/om100106e.
[27] G.M. Sheldrick, Crystal structure refinement with SHELXL, Acta Crystallogr. Sect. C Struct. Chem. 71 (2015) 3–8, http://dx.doi.org/10.1107/S2053229614024218.
[28] G.M. Sheldrick, A short history of SHELX, Acta Crystallogr. Sect. A Found. Crystallogr. 64 (2008) 112–122, http://dx.doi.org/10.1107/S0108767307043930.
[29] A.L. Spek, PLATON SQUEEZE: a tool for the calculation of the disordered solvent contribution to the calculated structure factors, Acta Crystallogr. Sect. C Struct. Chem. 71 (2015) 9–18, http://dx.doi.org/10.1107/S2053229614024929.
[30] A.K. Godwin, A. Meister, P.J. O'Dwyer, C.S. Huang, T.C. Hamilton, M.E. Anderson, High resistance to cisplatin in human ovarian cancer cell lines is associated with marked increase of glutathione synthesis, Proc. Natl. Acad. Sci. U. S. A. 89 (1992) 3070–3074, http://dx.doi.org/10.1073/pnas.89.7.3070.
[31] P.S. Pregosin, Platinum-195 nuclear magnetic resonance, Coord. Chem. Rev. 44 (1982) 247–291, http://dx.doi.org/10.1016/S0010-8545(00)80523-8.
[32] B.M. Still, P.G.A. Kumar, J.R. Aldrich-Wright, W.S. Price, ^{195}Pt NMR—theory and

application, Chem. Soc. Rev. 36 (2007) 665–686, http://dx.doi.org/10.1039/B606190G.
[33] S.J.S. Kerrison, P.J. Sadler, ^{195}Pt NMR studies of platinum(II) dimethylsuphoxide complexes, Inorg. Chim. Acta 104 (1985) 197–201, http://dx.doi.org/10.1016/S0020-1693(00)86771-7.
[34] P.S. Pregosin, E. Steiner, ^{15}N-NMR. A method for assigning structure in complexes of unsymmetrical *o*,*o*'-dihydroxydiarylazo-ligands, Helv. Chim. Acta. 59 (1976) 376–379, http://dx.doi.org/10.1002/hlca.19760590205.
[35] R.M. Gschwind, M. Armbrüster, I.Z. Zubrzycki, NMR detection of intermolecular NH···OP hydrogen bonds between guanidinium protons and bisposphonate moieties in an artificial arginine receptor, J. Am. Chem. Soc. 126 (2004) 10228–10229, http://dx.doi.org/10.1021/ja0483701.
[36] C. Deo, H. Wang, N. Bogliotti, Y. Zang, P. Retailleau, X.P. He, J. Li, J. Xie, Photoswitchable arene ruthenium and pentamethylcyclopentadienyl rhodium complexes containing *o*-sulfonamide azobenzene ligands: synthesis, characterization and cytotoxicity, J. Organomet. Chem. 820 (2016) 111–119, http://dx.doi.org/10.1016/j.jorganchem.2016.07.009.
[37] V.A. Kogan, S.G. Kochin, A.S. Antsyshkina, G.G. Sadikov, A.D. Garnovskii, The first experimental evidence for the *cis–trans* isomerism of metal chelates with oxyazo ligands, Mendeleev Commun. 9 (1999) 82–83, http://dx.doi.org/10.1070/MC1999v009n02ABEH001077.
[38] J. Griffiths II, Photochemistry of azobenzene and its derivatives, Chem. Soc. Rev. 1 (1972) 481–493, http://dx.doi.org/10.1039/cs9720100481.
[39] S. Steinwand, T. Halbritter, D. Rastädter, J.M. Ortiz-Sánchez, I. Burghardt, A. Heckel, J. Wachtveitl, Ultrafast spectroscopy of hydroxy-substituted azobenzenes in water, Chem.–Eur. J. 21 (2015) 15720–15731, http://dx.doi.org/10.1002/chem.201501863.
[40] C. Deo, N. Bogliotti, P. Retailleau, J. Xie, Triphenylphosphine photorelease and induction of catalytic activity from ruthenium-arene complexes bearing a photoswitchable*o*-tosylamide azobenzene ligand, Organometallics 35 (2016) 2694–2700, http://dx.doi.org/10.1021/acs.organomet.6b00431.
[41] M.D. Hall, K.A. Telma, K.E. Chang, T.D. Lee, J.P. Madigan, J.R. Lloyd, I.S. Goldlust, J.D. Hoeschele, M.M. Gottesman, Say no to DMSO: dimethylsulfoxide inactivates cisplatin, carboplatin, and other platinum complexes, Cancer Res. 74 (2014) 3913–3922, http://dx.doi.org/10.1158/0008-5472.CAN-14-0247.
[42] H. Huang, N. Humbert, V. Bizet, M. Patra, H. Chao, C. Mazet, G. Gasser, Influence of the dissolution solvent on the cytotoxicity of octahedral cationic Ir(III) hydride complexes, J. Organomet. Chem. 839 (2017) 15–18, http://dx.doi.org/10.1016/j.jorganchem.2016.12.010.
[43] S.F. Bellon, J.H. Coleman, S.J. Lippard, DNA unwinding produced by site-specific intrastrand cross links of the antitumor drug *cis*-diamminedichloroplatinum(II), Biochemistry 30 (1991) 8026–8035, http://dx.doi.org/10.1021/bi00246a021.
[44] M.V. Keck, S.J. Lippard, Unwinding of supercoiled DNA by platinum-ethidium and related complexes, J. Am. Chem. Soc. 114 (1992) 3386–3390, http://dx.doi.org/10.1021/ja00035a033.
[45] K.S. Lovejoy, R.C. Todd, S. Zhang, M.S. McCormick, J.A. D'Aquino, J.T. Reardon, A. Sancar, K.M. Giacomini, S.J. Lippard, *cis*-Diammine(pyridine)chloroplatinum(II), a monofunctional platinum(II) antitumor agent: uptake, structure, function, and prospects, Proc. Natl. Acad. Sci. U. S. A. 105 (2008) 8902–8907, http://dx.doi.org/10.1073/pnas.0803441105.
[46] J.-P. Macquet, J.-L. Butour, A circular dichroism study of DNA. platinum complexes. Differentiation between monofunctional, *cis*-bidentate and *trans*-bidentate platinum fixation on a series of DNAs, Eur. J. Biochem. 83 (1978) 375–387, http://dx.doi.org/10.1111/j.1432-1033.1978.tb12103.x.
[47] V. Brabec, V. Kleinwächter, J.-L. Butour, N.P. Johnson, Biophysical studies of the modification of DNA by antitumour platinum coordination complexes, Biophys. Chem. 35 (1990) 129–141, http://dx.doi.org/10.1016/0301-4622(90)80003-P.
[48] G.Y. Park, J.J. Wilson, Y. Song, S.J. Lippard, Phenanthriplatin, a monofunctional DNA-binding platinum anticancer drug candidate with unusual potency and cellular activity profile, Proc. Natl. Acad. Sci. U. S. A. 109 (2012) 11987–11992, http://dx.doi.org/10.1073/pnas.1207670109.
[49] T.C. Johnstone, J.J. Wilson, S.J. Lippard, Monofunctional and higher-valent platinum anticancer agents, Inorg. Chem. 52 (2013) 12234–12249, http://dx.doi.org/10.1021/ic400538c.